International Journal of Power Electronics and Drive System (IJPEDS)
Vol. 17, No. 4, December 2026, pp. 3054∼3061
ISSN: 2088-8694, DOI: 10.11591/ijpeds.v17.i4.pp3054-3061

IoT-based laser sensor for portable liquid-level monitoring

Alaa A. Al-Dhalemi, Ahmed Naser Al-Zurfi, Amer A. Chlaihawi, Ameen M. Al-Modaffer
Department of Electrical Engineering, Faculty of Engineering, University of Kufa, Najaf, Iraq

Article Info

Article history:

Received Jan 7, 2026
Revised Sep 10, 2026
Accepted Sep 17, 2026

Keywords:

Buoyancy float
Internet of things
Laser sensor
Liquid level
Mobile tank
Vibration robustness

ABSTRACT

This paper presents an internet of things (IoT)-based laser measurement system for monitoring liquid levels in fixed or mobile tanks. A Class II, 635-nm laser sensor is mounted above the tank and directed toward a tube-guided buoyancy float. An ESP32 processes the measurements, transmits them through MQTT, and displays the liquid level on a web interface in real time, while an MPU6050 records tank inclination. Laboratory evaluation included a separate static distance check, a synchronized filling test, a fixed-level vibration test, and a gradual tilt test. The static check produced errors of 0.478% for the laser sensor and 12.03% for the ultrasonic sensor at a tape-reference distance of 4.180 m. During the filling test, the laser residual standard deviation remained approximately 1.7 mm, whereas that of the ultrasonic sensor increased from 5.1 to 15.7 mm as the vibration level increased. These results show that, under the evaluated laboratory conditions, the guided-float laser assembly provided lower disturbance-related fluctuation than the co-located ultrasonic assembly.

This is an open access article under the CC BY-SA license.

Corresponding Author:

Amer A. Chlaihawi
Department of Electrical Engineering, Faculty of Engineering, University of Kufa
Najaf, Iraq
Email: amera.chlaihawi@uokufa.edu.iq

1. INTRODUCTION

Continuous liquid-level measurement underpins safe operation, efficient pumping, resource accounting, and regulatory compliance in petrochemical refineries, chemical-storage facilities, mobile fuel tanks, and water-supply networks [1]–[3]. It is also directly relevant to power-electronics and electric-drive systems: converter and motor-drive cooling loops must be monitored to avoid thermal runaway, steer-by-wire hydraulic actuators depend on reliable fluid-level feedback, and battery- or fuel-cell-vehicle systems require coolant/electrolyte level instrumentation, as illustrated by ESP32-based electric vehicle (EV) battery-monitoring platforms [4]. Internet of things (IoT) growth has enabled smart, autonomous, real-time process monitoring across these domains, reducing manual intervention and measurement error [4]–[6].

Existing technologies face different challenges in hazardous or dynamic environments. Electrical and mechanical sensors risk sparking in conductive, flammable or explosive atmospheres [7], [8]. Ultrasonic sensors suffer angle-dependent inaccuracy and wall-echo interference, especially where vibration and tilt disturb the acoustic path, as in vehicle fuel tanks or shipboard storage [8], [9]. Pressure transducers require liquid contact and are density-sensitive [10]; capacitive sensors struggle with non-dielectric or conductive liquids [11]. Optical-fiber sensors – fiber bragg grating (FBG) [12], [13], long-period grating [14], Mach–Zehnder [15], D-shaped [16], and macro-bending/sandwich-structure fibers [17]–[19] – offer high sensitivity and electromagnetic interference (EMI) immunity but are fragile and range-limited, well under 1 m [20]. Flange-type laser sensors reach sub-mm resolution to 1 m [21]; ToF rangefinders resolve ∼0.1 mm over tens of metres at higher cost [22]; portable POF sensors remain range-limited [23]. Low-cost ESP32-based IoT

platforms are widely validated for embedded sensing [3], [24], [25] including a LoRa-based buoyancy level sensor [25] and a laser-and-inertial-unit system with machine learning [26] – but neither is validated under both vibration and tilt with IoT/MQTT connectivity, a combination that, to our knowledge, remains unreported.

This gap motivates a low-cost, guided-float laser/IoT system for operation under vibration and tilt, where ultrasonic measurement can degrade [8], [9]. The novelty lies in system integration and the experimental validation protocol rather than individual components: i) a tube-guided, self-centering float measured by a Class II laser, ii) ESP32/MQTT-based web monitoring, and iii) vibration and tilt characterization from logged raw-data statistics. Contributions include the guided-float optical readout, real-time IoT visualization, quantitative σ/MAE/RMSE/SEM analysis, and comparison with recent IoT-based and optical level-sensing systems, using a 550-mm filling apparatus and a separate static check at $\sim$4.2 m (Table 1).

Table 1. Comparison of liquid-level sensing technologies with the proposed system

Parameter	Flange-type [21]	Laser ToF [22]	FPI fiber-optic [12]	Proposed
Technology	Laser reflection	ToF / phase-shift	F-P interferometer	Laser reflection (float-guided)
Resolution	$\sim$1 mm	$\sim$0.1 mm	$\sim \mu$m	$\sim$1 mm (datasheet)
Range	0.1–5 m	0.05–20 m	0–1 m	0.55-m filling setup; $\sim$4.2 m static check
IoT capability	Moderate	High	Low	High
Cost	Low–moderate	Moderate–high	High	Low–moderate
Error (%)	$\sim$2–5	$<$1	$<$0.5	0.478%
Mobile-tank compatible	Yes	Yes (with damping)	No	Vibration- and tilt-tested
Supply voltage (V DC)	5–24	12–24	3.3–5	2.0–3.3
Temp. range	$-$20 to 60 °C	$-$10 to 50 °C	10 to 40 °C	0 to 40 °C

Note: Values are reported from the cited studies or corresponding device specifications. Direct comparison is limited by differences in sensor configurations and experimental conditions

2. METHOD

The proposed system follows an experimental design that combines a hardware prototype with real-time IoT data acquisition, organized into five functional phases: i) optical distance sensing via a Class II laser distance module, ii) data acquisition and wireless communication by the ESP32, iii) a mechanical tank structure with a buoyancy-based float, iv) system logic control, and v) real-time web visualization. Figure 1 shows the complete schematic of the measurement setup, including the labeled geometry (H, H_o, S_o, E) used to compute the liquid level from the sensor readings.

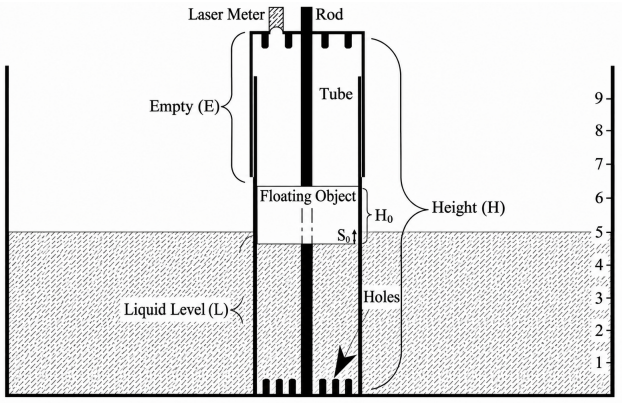

Figure 1. Schematic of the proposed IoT-based laser liquid-level measurement system

2.1. Hardware: laser module, ESP32, and float assembly

The proposed system integrates a Class II laser distance module, an ESP32 microcontroller, an MPU6050 sensor, and a tube-guided buoyant float. The laser measures the distance to the reflective float surface, providing a non-contact optical readout; the ESP32 acquires the laser and tilt data, computes the liquid level using (3), and publishes it via message queuing telemetry transport (MQTT) – consistent with widely validated ESP32-based IoT sensing [4], [24] and with optical liquid-level sensing in harsh environments and Archimedes-buoyancy configurations [27], [28].

The vertical guide pipe is connected to the tank at its base, so that the liquid level inside the pipe follows the tank level. A cylindrical float moves along a central stabilizing rod, which limits lateral displacement during vibration and tilt. The laser therefore measures the float position without making direct contact with the liquid. The hardware and communication specifications are summarized in Table 2.

2.2. Mathematical model: archimedes' buoyancy principle

The floating mechanism is governed by Archimedes' buoyancy principle [12], [28]: at equilibrium, the buoyant force acting on the submerged portion of the float equals the float's weight,

$$\rho_L V_{ps} g = \rho_o V_o g \quad \Rightarrow \quad \rho_L V_{ps} = \rho_o V_o, \tag{1}$$

where ρ_L, ρ_o are the liquid and float densities and V_{ps}, V_o are the submerged and total float volumes. For a cylindrical float of radius r, $V_{ps} = \pi r^2 S_o$ and $V_o = \pi r^2 H_o$, giving (2).

$$S_o = H_o \left(\frac{\rho_o}{\rho_L} \right) \tag{2}$$

The liquid level is then computed from the laser-measured distance E (module to float top). With the float's exposed height equal to $H_o - S_o$, the level relative to the pipe base is (3).

$$L = H - E - (H_o - S_o) = H - E - H_o + S_o. \tag{3}$$

The (3) follows directly from the geometry in Figure 1 and is used throughout the analysis and Algorithm 1.

2.3. Accuracy and dispersion metrics

Measurement accuracy is quantified using the conventional percentage-error expression, with the independent reference value V_A in the denominator: $\delta = |(V_E - V_A)/V_A| \times 100$, where V_E is the sensor reading. Independently of the 550-mm filling apparatus, a separate static sensor-distance check was performed using a manual measuring tape ($V_A = 4.180$ m, the reference), the laser module ($V_{E,\text{laser}} = 4.200$ m), and the ultrasonic sensor ($V_{E,\text{ultrasonic}} = 4.683$ m), giving (4).

$$\delta_{\text{laser}} = \left| \frac{4.200 - 4.180}{4.180} \right| \times 100 = 0.478\%, \qquad \delta_{\text{ultrasonic}} = \left| \frac{4.683 - 4.180}{4.180} \right| \times 100 = 12.03\%. \tag{4}$$

Both errors were calculated against the same tape reference. To assess measurement fluctuation under dynamic conditions, distance readings from both sensors were recorded synchronously at $\sim$1 Hz during a tank-filling run spanning low vibration (the first $\sim$40 s of the 188-sample record) and medium/high vibration (the remaining $\sim$150 s). Because the true level changes continuously during filling, each sensor's own smooth trend was estimated with a Savitzky–Golay filter (2nd-order, 11-sample window), and the residual $r_i = x_i - \hat{x}_i$ was used as an indicator of disturbance-related fluctuation. Dispersion metrics were computed from these residuals calculated as (5).

$$\text{RMSE} = \sqrt{\tfrac{1}{N} \textstyle\sum r_i^2}, \quad \text{MAE} = \tfrac{1}{N} \textstyle\sum |r_i|, \quad \sigma = \sqrt{\tfrac{1}{N-1} \textstyle\sum (r_i - \bar{r})^2} \tag{5}$$

These statistics were computed from the complete logged dataset. Separate fixed-level vibration and tilt tests were also performed, with the corresponding results reported as observed variation bands.

2.4. Control algorithm and experimental setup

The ESP32 firmware implements the acquisition and alarm logic shown in Algorithm 1. It requests a distance reading, computes L using (3), and, when Wi-Fi is connected, publishes L over MQTT and triggers a low-level alarm if $L \leq L_{\min}$. When disconnected, it buffers the data locally and raises a communication-failure alarm after $T_{\max}$ cycles.

The system was built and evaluated in the Electrical Engineering Laboratory, University of Kufa, Najaf, Iraq. Figure 2(a) shows the physical assembly – a transparent glass tank with the laser-guided float/pipe on the right, a co-located ultrasonic reference sensor/float on the left, and the MPU6050/ESP32 mounted above, each component labeled; Figure 2(b) shows the data-acquisition chain (Wi-Fi router, wiring, and the laptop running the logging terminal). Table 2 lists the hardware and protocol specifications. Both sensors were functionally checked against manual tape measurements at several tank heights before each test; the quantitative accuracy result reported here reflects an independent spot check from that comparison.

The system was validated using 3 protocols: i) a static sensor-distance check against an independent tape reference, followed by a synchronized filling run comparing laser and ultrasonic measurements; ii) a fixed-level vibration test – manual lateral taps for "low" and more vigorous sustained shaking for "medium/high," each held for the full logging window; and iii) a tilt test, with a manually operated hinged base raising α from 0° to $\sim 20^\circ$ while the MPU6050 logged inclination. Performance was assessed via the percentage-error spot check, residual dispersion metrics where logged, and observed stability bands otherwise.

Algorithm 1 ESP32 measurement, communication, and alarm algorithm

Require: H, H_o, S_o (geometry); $L_{\min}$ (low-level threshold); $T_{\max}$ (Wi-Fi timeout limit)
Ensure: streamed level $L(t)$; low-level alarm; connectivity status; communication-failure alarm

$T \leftarrow 0$; $CommFailureLatched \leftarrow$ false
loop
  READDISTANCE; $E \leftarrow$ PARSEDISTANCEREPLY
  $L \leftarrow H - E - H_o + S_o$ ▷ (3)
  if ISWIFICONNECTED **then**
    $T \leftarrow 0$; $CommFailureLatched \leftarrow$ false
    if $L \leq L_{\min}$ **then**
      SENDALARMLOWLEVEL
    end if
    PRINTANDSEND(L) ▷ MQTT publish
  else
    PRINTNOTCONNECTED; BUFFERLOCALLY(L); $T \leftarrow T + 1$
    if $T \geq T_{\max}$ **and not** $CommFailureLatched$ **then**
      ATTEMPTRECONNECT; SENDALARMCOMMFAILURE; $CommFailureLatched \leftarrow$ true
    end if
  end if
  if POWEROFFCOMMANDRECEIVED **then**
    break
  end if
end loop



(a) (b)

Figure 2. Experimental setup: (a) tank and sensor assembly and (b) data-acquisition and IoT communication setup

Table 2. Hardware and protocol specifications

Item	Specification
Laser module	JRT B707C; 635 nm; $<$ 1 mW; Class II; UART, 19200 bps, 8N1
Ultrasonic module	HC-SR04; 40 kHz; trigger/echo GPIO; 5 V to 3.3 V level shifting
Microcontroller	ESP32-WROOM-32; dual-core Xtensa LX6; Wi-Fi 802.11 b/g/n
IMU	MPU6050; 6-axis gyro/accelerometer; I^2C; 3.3 V
MQTT broker	Mosquitto; local laptop host; TCP port 1883; $\sim$1 Hz
Sampling interval	1000 ms nominal loop; 188 samples in $\sim$190 s
Guide-pipe height	$H \approx 550$ mm
Pipe/float dimensions	Pipe ID 10 cm; float diameter 9 cm; height 2 cm; mass 6 g

3. RESULTS AND DISCUSSION

3.1. Sensor calibration and static filling results

Figure 3 shows the synchronized filling-test record acquired over approximately 190 s, with low vibration during the first ∼40 s and medium-to-high vibration thereafter. As the tank fills and the float rises, the measured sensor distance decreases from about 530 to about 120 mm. The laser trace (solid line, circular markers) follows this trend closely, whereas the ultrasonic trace (dashed line, triangular markers) shows greater scatter, especially after $t \approx 40$ s. Distinct line styles and marker shapes, rather than color alone, keep the figure legible in grayscale.

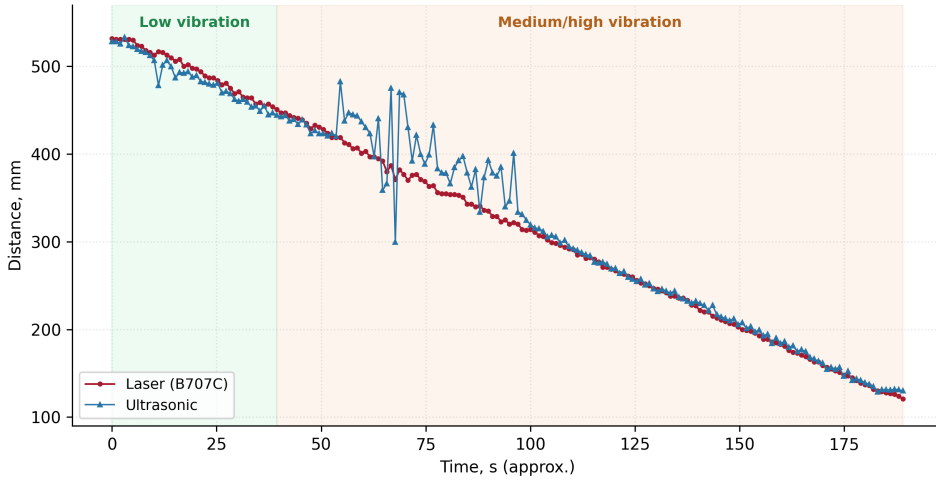

Figure 3. Laser and ultrasonic distance measurements during the filling test

3.2. Vibration analysis

Table 3 reports the fluctuation statistics from the logged measurements in Figure 3. Because the true level changed continuously during filling, each sensor's trend was estimated separately with a second-order Savitzky–Golay filter (11-sample window), and σ, mean absolute error (MAE), root mean square error (RMSE) and standard error of the mean (SEM) were computed from the resulting residuals for each vibration segment. Under low vibration, the laser channel's residual $\sigma \approx 1.7\,\mathrm{mm}$ versus $\sigma \approx 5.1\,\mathrm{mm}$ for the ultrasonic channel; under medium-to-high vibration the laser σ remained $\approx 1.7\,\mathrm{mm}$ while the ultrasonic σ rose to $\approx 15.7\,\mathrm{mm}$. These residuals measure fluctuation, not absolute accuracy. The guided-float laser assembly was thus less affected by disturbance than the co-located ultrasonic assembly, consistent with the reported sensitivity of ultrasonic ranging to angular misalignment and wall echoes [8], [9].

A separate fixed-level vibration test and a gradual tank-tilt test (0° to ∼20°, inclination recorded by the MPU6050) were also conducted, with results displayed on the system's real-time dashboard (radial and digital gauges updated over MQTT). Under fixed-level vibration, the laser stayed within an observed ±5 mm band versus ±25 mm with several large transient spikes for the ultrasonic sensor. Under gradual tilt, the laser stayed within ±8 mm while the ultrasonic sensor showed markedly larger scatter, with outliers exceeding 30 mm from the mean trend (Figure 4) – observed extrema consistent with the dispersion pattern in Table 3.

Table 3. Savitzky–Golay detrended-residual statistics for the filling test

Segment	Metric (mm)	Laser	Ultrasonic
Low vibration ($n = 40$)	σ	1.7	5.1
	MAE	1.5	3.2
	RMSE	1.7	5.0
	SEM	0.27	0.81
Medium/high vibration ($n = 148$)	σ	1.7	15.7
	MAE	1.2	7.1
	RMSE	1.7	15.7
	SEM	0.14	1.29

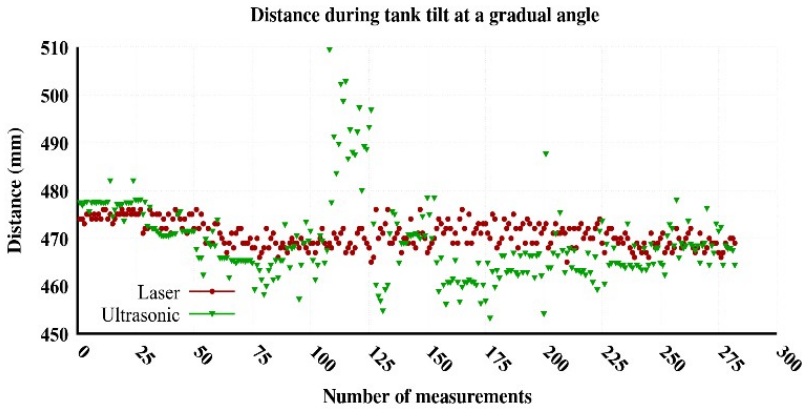

Figure 4. Laser and ultrasonic measurements during gradual tank tilt from 0° to 20°

3.3. Real-time IoT visualization and remote monitoring

The web-based interface enables remote liquid-level monitoring through an HTML page with real-time radial and digital gauges updated via MQTT. Configurable alert thresholds trigger push notifications when the liquid level approaches predefined minimum or maximum values. The communication and alarm functions follow the algorithm-level buffering and latched-alarm logic of Algorithm 1, in the spirit of threshold-triggered IoT alerting reported for other smart-tank platforms [6], [25].

Relative to the flange-type laser sensor [21], the proposed system adds direct IoT integration and vibration/tilt characterization not reported there. Its 0.478% spot-check error compares favorably with artificial neural network (ANN)-based adaptive ultrasonic systems reporting $\sim$1 cm error over 500 cm [9]. Pressure-based sensors require liquid contact and are sloshing-sensitive [10]; portable POF sensors [23] need precise alignment and a limited range; ToF rangefinders [22] and FBG buoyancy sensors [12], [28] achieve high resolution but lack the raw-data-based dynamic noise analysis in Table 3. Unlike tilt-compensated systems using auxiliary sensor fusion [29] or IoT buoyancy sensors validated only under static/slow-varying conditions [25], the present system characterizes both vibration- and tilt-induced disturbance directly from logged raw-data statistics – demonstrating competitive dynamic stability among the surveyed technologies (Table 1).

4. CONCLUSION

This study experimentally evaluated an IoT-connected, guided-float Class II laser sensor with ESP32/MQTT communication and MPU6050 tilt monitoring. A single-point tape-reference check yielded errors of 0.478% (laser) and 12.03% (ultrasonic). Across the paired filling-test measurements, the laser residual standard deviation remained near 1.7 mm, while the ultrasonic sensor's rose from 5.1 to 15.7 mm as vibration increased. In the fixed-level vibration test, the observed variation bands were ± 5 mm (laser) and ± 25 mm (ultrasonic); the laser stayed within ± 8 mm during the tilt test. The σ, MAE, RMSE and SEM results indicate the guided-float laser assembly is less disturbance-sensitive than the co-located ultrasonic assembly, and the proposed configuration is suitable for real-time liquid-level monitoring under the evaluated vibration and tilt conditions. The study is limited to laboratory testing; repeated trials, uncertainty analysis, and industrial validation remain future work.

FUNDING INFORMATION

Authors state no funding involved.

AUTHOR CONTRIBUTIONS STATEMENT

This journal uses the Contributor Roles Taxonomy (CRediT) to recognize individual author contributions, reduce authorship disputes, and facilitate collaboration.

Name of Author	C	M	So	Va	Fo	I	R	D	O	E	Vi	Su	P	Fu
Alaa A. Al-Dhalemi	✓	✓	✓	✓	✓	✓		✓	✓	✓			✓	
Ahmed Naser Al-Zurfi		✓	✓		✓					✓				
Amer A. Chlaihawi		✓				✓		✓	✓	✓	✓	✓		
Ameen M. Al-Modaffer				✓	✓		✓			✓		✓		

C : **C**onceptualization
M : **M**ethodology
So : **So**ftware
Va : **Va**lidation
Fo : **Fo**rmal Analysis
I : **I**nvestigation
R : **R**esources
D : **D**ata Curation
O : Writing - **O**riginal Draft
E : Writing - Review & **E**diting
Vi : **Vi**sualization
Su : **Su**pervision
P : **P**roject Administration
Fu : **Fu**nding Acquisition

CONFLICT OF INTEREST STATEMENT

Authors state no conflict of interest.

DATA AVAILABILITY

The datasets (raw sensor logs and derived statistics) generated and analyzed during the current study were used for the purposes of this study only and are not otherwise publicly available.

REFERENCES

[1] Z. Liu, Q. Fan, J. Liu, L. Zhou, and Z. Zhang, "Robust intelligent monitoring and measurement system toward downhole dynamic liquid level," *Sensors*, vol. 24, no. 11, Jun. 2024, doi: 10.3390/s24113607.

[2] V. Shenoy, P. Shenoy, and S. K. Venkata, "Accurate liquid level measurement with minimal error: a chaotic observer approach," *Computation*, vol. 12, no. 2, Feb. 2024, doi: 10.3390/computation12020029.

[3] M. A. Wister, E. Leon, A. Alejandro-Carrillo, P. Pancardo, and J. A. Hernandez-Nolasco, "Using IoT for cistern and water tank level monitoring," *Applied System Innovation*, vol. 7, no. 6, Nov. 2024, doi: 10.3390/asi7060112.

[4] E. Gomez-Huaylla, L. Mejía-Cruz, and E. Paiva-Peredo, "Management and monitoring of lithium-ion battery recharge with ESP32," *International Journal of Power Electronics and Drive Systems (IJPEDS)*, vol. 15, no. 3, Sep. 2024, doi: 10.11591/ijpeds.v15.i3.pp1677-1686.

[5] S. Kumar, P. Tiwari, and M. Zymbler, "Internet of things is a revolutionary approach for future technology enhancement: a review," *Journal of Big Data*, vol. 6, no. 1, Dec. 2019, doi: 10.1186/s40537-019-0268-2.

[6] F. Jan, N. Min-Allah, S. Saeed, S. Z. Iqbal, and R. Ahmed, "IoT-based solutions to monitor water level, leakage, and motor control for smart water tanks," *Water*, vol. 14, no. 3, Jan. 2022, doi: 10.3390/w14030309.

[7] Z. Wang, Z. Tan, R. Xing, L. Liang, Y. Qi, and S. Jian, "Liquid level sensor based on fiber ring laser with single-mode-offset coreless-single-mode fiber structure," *Optics & Laser Technology*, vol. 84, pp. 59–63, Oct. 2016, doi: 10.1016/j.optlastec.2016.05.001.

[8] P. Mohindru, "Development of liquid level measurement technology: A review," *Flow Measurement and Instrumentation*, vol. 89, Mar. 2023, doi: 10.1016/j.flowmeasinst.2022.102295.

[9] A. K. Sahoo and S. K. Udgata, "A novel ANN-based adaptive ultrasonic measurement system for accurate water level monitoring," *IEEE Transactions on Instrumentation and Measurement*, vol. 69, no. 6, pp. 3359–3369, Jun. 2020, doi: 10.1109/TIM.2019.2939932.

[10] P. Esmaili, F. Cavedo, and M. Norgia, "Characterization of pressure sensor for liquid-level measurement in sloshing condition," *IEEE Transactions on Instrumentation and Measurement*, vol. 69, no. 7, pp. 4379–4386, Jul. 2020, doi: 10.1109/TIM.2019.2945414.

[11] J. R. Hanni and S. K. Venkata, "A novel helical electrode type capacitance level sensor for liquid level measurement," *Sensors and Actuators A: Physical*, vol. 315, Nov. 2020, doi: 10.1016/j.sna.2020.112283.

[12] M. Consales *et al.*, "A fiber bragg grating liquid level sensor based on the Archimedes' Law of buoyancy," *Journal of Lightwave Technology*, vol. 36, no. 20, pp. 4936–4941, Oct. 2018, doi: 10.1109/JLT.2018.2866130.

[13] A. Leal-Junior, V. Biazi, C. Marques, and A. Frizera, "Force-displacement analysis in diaphragm-embedded fiber bragg grating sensors," *Sensors*, vol. 22, no. 14, Jul. 2022, doi: 10.3390/s22145355.

[14] M. Zhang *et al.*, "Power-type liquid-level sensor for high refractive index liquid based on long-period fiber grating," *Sensors and Actuators A: Physical*, vol. 324, Jun. 2021, doi: 10.1016/j.sna.2021.112652.

[15] T. Gabler *et al.*, "Investigation of liquids with microcavity in-line Mach-Zehnder interferometers – impact of the microcavity shape on the sensing performance," *Optical Fiber Technology*, vol. 73, Oct. 2022, doi: 10.1016/j.yofte.2022.103059.

[16] Y. Ying, G. Si, F. Luan, K. Xu, Y. Qi, and H. Li, "Recent research progress of optical fiber sensors based on D-shaped structure," *Optics & Laser Technology*, vol. 90, pp. 149–157, May 2017, doi: 10.1016/j.optlastec.2016.11.021.

[17] K. Liao, Y. Li, M. Lei, and X. Li, "A liquid level sensor based on spiral macro-bending plastic optical fiber," *Optical Fiber Technology*, vol. 70, May 2022, doi: 10.1016/j.yofte.2022.102874.

[18] X. Yang *et al.*, "Simultaneous measurement of liquid level and refractive index based on a sandwich multimode optical fiber structure," *Optics & Laser Technology*, vol. 168, Jan. 2024, doi: 10.1016/j.optlastec.2023.109856.

[19] O. Fuentes *et al.*, "Increasing the sensitivity of an optic level sensor with a wavelength and phase sensitive single-mode multimode single-mode fiber structure," *IEEE Sensors Journal*, vol. 17, no. 17, pp. 5515–5522, Sep. 2017, doi: 10.1109/JSEN.2017.2724849.

[20] M. Elsherif *et al.*, "Optical fiber sensors: working principle, applications, and limitations," *Advanced Photonics Research*, vol. 3, no. 11, Nov. 2022, doi: 10.1002/adpr.202100371.
[21] K. Suemori, Y. Komatsu, and T. Nobeshima, "Flange-type liquid-level sensor based on laser light reflection," *Sensors International*, vol. 4, 2023, doi: 10.1016/j.sintl.2023.100230.
[22] B. Brenneis, "Long range optical distance sensors for liquid metal free surface detection," *Journal of Nuclear Engineering*, vol. 3, no. 4, pp. 364–372, Nov. 2022, doi: 10.3390/jne3040023.
[23] M. S. U. K. Haider *et al.*, "Portable optical fiber sensor for continuous liquid level sensing using commercially available POF," *IEEE Sensors Journal*, vol. 25, no. 3, pp. 4582–4589, Feb. 2025, doi: 10.1109/JSEN.2024.3511929.
[24] D. Hercog, T. Lerher, M. Truntič, and O. Težak, "Design and implementation of ESP32-based IoT devices," *Sensors*, vol. 23, no. 15, Jul. 2023, doi: 10.3390/s23156739.
[25] B. Kim and S. Jang, "Design of IoT-based buoyancy-based level sensors for low-cost and high-efficiency," *Journal of Sensor Sciene and Technology*, vol. 33, no. 5, pp. 378–383, Sep. 2024, doi: 10.46670/JSST.2024.33.5.378.
[26] C. M. Ranieri *et al.*, "Water level identification with laser sensors, inertial units, and machine learning," *Engineering Applications of Artificial Intelligence*, vol. 127, Jan. 2024, doi: 10.1016/j.engappai.2023.107235.
[27] C. M. Petrie and J. L. McDuffee, "Liquid level sensing for harsh environment applications using distributed fiber optic temperature measurements," *Sensors and Actuators A: Physical*, vol. 282, pp. 114–123, Oct. 2018, doi: 10.1016/j.sna.2018.09.014.
[28] C. C. Ramos *et al.*, "High resolution liquid level sensor based on Archimedes' law of buoyancy using polymer optical fiber Bragg gratings," *Measurement*, vol. 252, Aug. 2025, doi: 10.1016/j.measurement.2025.117368.
[29] S.-L. Yun, P. J. Kwak, K. S. Kim, D. S. Choi, and H. J. Oh, "Development of a tilt-compensated smart water level measurement system for urban flood management," *Journal of Korean Society of Environmental Engineers*, vol. 47, no. 11, pp. 760–768, Nov. 2025, doi: 10.4491/KSEE.2025.47.11.760.

BIOGRAPHIES OF AUTHORS



Alaa A. Al-Dhalemi is a lecturer in the Department of Electrical Engineering, Faculty of Engineering, University of Kufa, Najaf, Iraq. He received the B.Sc. degree in electrical engineering from the University of Baghdad, Iraq, and the M.Sc. degree in computer and communication engineering, with a specialization in embedded systems, from Universiti Malaysia Perlis, Malaysia. His research interests include embedded systems, edge computing, robotics, computer vision, and artificial intelligence. He can be contacted at email: alaaa.aldhalemi@uokufa.edu.iq.



Ahmed Naser Al-Zurfi is a faculty member in the Electrical Engineering Department at the University of Kufa, Iraq. His research interests include sensor systems, signal processing, and IoT-based industrial monitoring. He has contributed to several applied research projects in instrumentation and control engineering. He can be contacted at email: ahmedn.alzurfi@uokufa.edu.iq.



Amer A. Chlaihawi is an assistant professor in the Electrical Engineering Department at the University of Kufa, Iraq. He received his B.Eng., M.Eng., and Ph.D. degrees in electrical engineering. His research interests include optical sensing, IoT systems, embedded electronics, and industrial process monitoring. He can be contacted at email: amera.chlaihawi@uokufa.edu.iq.

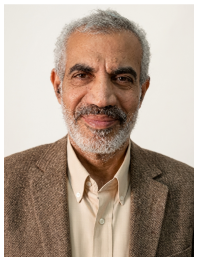

Ameen M. Al-Modaffer is a faculty member in the Electrical Engineering Department at the University of Kufa, Iraq. His research interests include control systems, measurement instrumentation, and IoT applications for industrial processes. He has participated in various experimental and applied research projects focused on smart sensing and automation.